Journal of Materials Chemistry A

Accepted Manuscript

ROYAL SOCIETY OF CHEMISTRY

www.rsc.org/materialsA

Journal Name

RSCPublishing

ARTICLE

Pyrite FeS_2 Microspheres Wrapped by Reduced Graphene Oxide as High-Performance Lithium-Ion Battery Anodes

Cite this: DOI: 10.1039/x0xx00000x

Received 00th January 2012,
Accepted 00th January 2012

DOI: 10.1039/x0xx00000x

www.rsc.org/

Hongtao Xue,[a, b, c] Denis Yu,[a, d] Jian Qing,[a, b] Xia Yang,[a, b] Jun Xu,[a, b] Zhangpeng Li,[a, b] Mingliang Sun,[a, b] Wenpei Kang,[a, b] Yongbing Tang,[a, b, e, *] and Chun-Sing Lee[a, b, *]

A composite of pyrite FeS_2 microspheres wrapped by reduced graphene oxide (FeS_2/rGO) has been synthesized by a facile one-step solvothermal method and applied as anode in lithium ion batteries (LIBs). Impedance measurements and transmission electron microscopy show that incorporation of rGO significantly decreases the charge transfer resistance and improves the structural stability of the composite. As an anode material for a LIB, the composite exhibits a high capacity of 970 mA h g^{-1} at a current density of 890 mA g^{-1} after 300 cycles. Additionally, this composite anode shows impressive performance especially at high current densities. The LIB shows a capacity of 380 mA h g^{-1} even at a high current density of 8900 mA g^{-1} (10 C) over 2000 cycles, demonstrating its potential for applications in LIBs with long cycling life and high power density.

Introduction,

Pyrite iron sulfide (FeS_2) is an interesting optical and electronic material for photovoltaic and energy storage applications due to their abundance in nature and inexpensive cost.[1-3] Pyrite has been investigated as counter electrode in photovoltaic devices, cathode or anode material in lithium batteries.[2-4] It is a promising lithium battery electrode material with a high theoretical capacity of 890 mAh g^{-1} assuming four electron transfer. Therefore, pyrite has been intensively investigated as the cathode or anode material.[3-5] Unfortunately, reduction of pyrite Fe_2S with lithium forms polysulfide Li_2S_x ($2<x<8$), which can easily dissolve into the liquid electrolytes and break the electrical contact between active material and current collector, leads to a poor cycle performance and hampers its practical LIBs application.[3-15] One strategy to address this problem is to design liquid electrolyte with special group for suppressing polysulfide dissolution.[3-5] Another effective approach is to wrap the electrode materials with polymer or carbon coating layer to effectively reduce the dissolution of polysulfide into the electrolyte, which significantly improved the rate and cycling capabilities.[10-34]

Recently, Song's group successfully synthesized iron sulfide-embedded carbon microspheres, which exhibited a high specific capacity of 736 mA h g^{-1} at a current rate of 50 mA g^{-1} after 50 cycles.[10] Xu et al. also reported a soft template approach to synthesize ultrathin carbon-coated FeS nanosheets, which have a discharge capacity of 615 mA h g^{-1} at a current of 100 mA g^{-1} after 100 cycles.[11] Son et al. embedded natural pyrite in a polyacrylonitrile matrix to enhance the electrochemical performance stability of the FeS_2 as cathode material, and this composite cathode showed a capacity of 470 mA h g^{-1} after 50 cycles.[12] Liu et al. also obtained carbon-encapsulated pyrite for LIB cathode; the discharge capacity remains about 500 mA h g^{-1} after 50 cycles.[13] While the high capacities reported in these earlier works clearly suggested that carbon-coated pyrite has good potential for LIB application, long-term stability at high current rate has to be investigated to enable its commercialization.

Recent studies in Li-S battery showed that wrapping the sulfur into graphene sheets can significantly reduce the dissolution of polysulfide into the electrolyte and improve the cycling stability and rate performance.[20-29] We therefore adopt a similar strategy to wrap FeS_2 with a thin layer of graphene to reduce Li_2S_x dissolution into the organic electrolyte. Here, we report the synthesis of pyrite FeS_2 microspheres/reduced graphene oxide (FeS_2/rGO) composites *via* a facile solvothermal approach. For practical application, micrometers FeS_2 structures are more easily to industrial production and processing as well as a higher packing density for lithium battery. As the anode of LIB, this composite exhibits a capacity of ~1000 mA h g^{-1} at a current density of 890 mA g^{-1} after 300 cycles. Moreover, it retains a capacity of 380 mA h g^{-1} even at a high current density

of 8900 mA g^{-1} (10C) after 2000 cycles, demonstrating its potential applications for LIBs with long cycling life and high power density.

Experimental

Synthesis of FeS_2/rGO Composite

Graphene oxide (GO) was prepared by a modified Hummer method.[34-36] In brief, graphite (3.0 g) was mixed with $NaNO_3$ (1.5 g), concentrated H_2SO_4 (69 mL) and $KMnO_4$ (9.0 g), and the mixture was cooled in an ice bath under vigorous stirring for 30 min. The reaction was then heated to 35 °C and stirred for 30 min. Afterwards, deionized water (138 mL) was dropped slowly into the solution for 30 min. Additional water (420 mL) and H_2O_2 (30%, 3 mL) was added and the mixture was kept at 98 °C for 15 min. After cooling in ambient temperature, the mixture was filtered and washed for several times with diluted HCl aqueous solution (200 mL, 30 wt%), water and ethanol. The obtained yellow-brown solid was then dispersed in water by ultrasonication at room temperature for 1 hour.

For synthesis of FeS_2/rGO composites, a mixture of the as-prepared GO solution (2 mL, 9 mg/mL), $FeSO_4$•$7H_2O$ (3 mmol) and sulfur (7 mmol) powder were added in triethylene glycol (TEG, 100 mL) and ultrasonicated for 30 min. The mixed solution was kept at 200 °C for 20 hours. After cooling to room temperature in air, the reaction product was collected and washed with distilled water and ethanol several times, and then dried under vacuum. The final product was annealed in N_2 gas at 400 °C for 30 minutes. For comparison, the FeS_2 sample, which we call bare FeS_2, prepared without GO was also obtained in the same way.

Characterization

The as-prepared samples were characterized by scanning electron microscopy (SEM) and transmission electron microscopy (TEM) with a Philips XL30 FEG SEM and a Philips CM200 FEG TEM (operating at 200 kV), respectively. X-ray diffraction (XRD) was carried out with Philips X'Pert diffractometer using Cu Kα radiation. Raman measurements were conducted using a Renishaw 2000 laser Raman microscope equipped with a 514 nm argon ion laser of 2 mm spot size for excitation. Electrochemical impedance spectroscopy (EIS) measurements were performed using an impedance measurement unit (ZAHNER-elektrik IM6) with an AC amplitude of 10 mV and a frequency range of $0.1–10^5$ Hz.

Test coin cells were assembled in a dry argon-filled glove box with the working electrode consisted of FeS_2/rGO (80%), Carbon black (10%), and CMC (carboxymethyl cellulose, 10%) on the copper foil. Pure metallic lithium foil served as a counter electrode. The separator was one layer of a polypropylene glycol film (Celgard 2025). The electrolyte was 1 M $LiPF_6$ dissolved in an ethylene carbonate (EC)/dimethyl carbonate (DMC) mixture (1:1 in volume). Cyclic voltammetry (CV) measurements were carried out with a CHI660C electrochemical workstation. Galvanostatic charge-discharge experiments were carried out with a MACCO Instruments system.

Results and discussion,

The preparation of the microspheres FeS_2/rGO composite is schematically illustrated in Fig. 1. The synthesized GO sheets dispersed in water are negatively charged due to the ionization of carboxyl and hydroxyl groups on their surface.[30] The positively charged Fe^{2+} ions will be absorbed on the surface of GO sheets by electrostatic attraction. The solvothermal reaction results in the formation of the FeS_2 on graphene oxide. The sulfur powder provides the sulfur atoms which nucleate with the Fe^{2+} ions to form FeS_2. The formed FeS_2 will self assemble into the ball-like microspheres to decrease the surface energy while the graphene oxide is partially reduced. Finally, the composite of FeS_2 microspheres warped by the rGO sheets was formed by the solvothermal process.

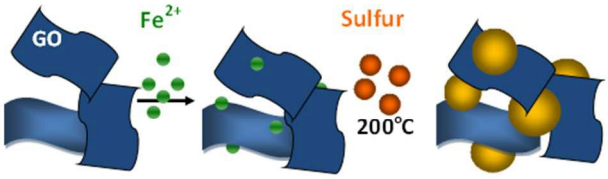

Fig. 1. Schematic illustration of the FeS_2/rGO composite by solvothermal synthesis.

Fig. 2a shows an SEM image of the as-prepared FeS_2 sample obtained without addition of rGO in the preparation. It can be seen that the formed microspheres have a uniform ball-like morphology with diameter of 1-3 μm. When rGO is added in the reaction system while keeping other conditions unchanged, the synthesized microspheres are wrapped by the reduced graphene oxide sheets, as shown in Fig. 2b. Microstructure of the composite was further studied with TEM and high-resolution TEM (HRTEM). Fig. 2c shows a TEM image of a typical microsphere with rGO sheets wrapping on the surface. The inset in Fig. 2c displays an HRTEM image, from which the lattice spacings of 0.27 and 0.24 nm match well respectively with those of the (200) and the (210) planes of pyrite FeS_2.

XRD diffraction patterns of the synthesized samples with and without using GO are shown in Fig. 2d. The two samples exhibit similar XRD pattern, all diffraction peaks can be readily indexed to a cubic lattice of pyrite FeS_2 (JCPDF card No. 42-1340, space group *Pa-3*, *a = 5.419 Å*). Fig. 2e shows a Raman spectrum of the FeS_2/rGO composites. There are two strong feature peaks at 335 and 376 cm^{-1} as well as a weak peak at 423 cm^{-1}, which match well respectively with the reported values of the E_g, A_g, and T_g modes of pyrite FeS_2.[37-38] There are no obvious vibration peaks in the range of 200-300 cm^{-1} from Fe_xS or Fe_xO. Two strong peaks at 1348 and 1582 cm^{-1} correspond to the D band and the G band of rGO, respectively.[39]

Thermo-gravimetric analysis (TGA) curves of the FeS_2 and the FeS_2/rGO samples are shown in Fig. 2f. The TGA measurements were carried out under an oxygen atmosphere. There is a significant difference in their thermal oxidative degradation characteristics. The thermal degradation of FeS_2/rGO composite undergoes two major weight loss stages, while that of FeS_2 shows three major stages. From the TGA curve of the FeS_2/rGO composite, the content of graphene is about 9.6 wt%.

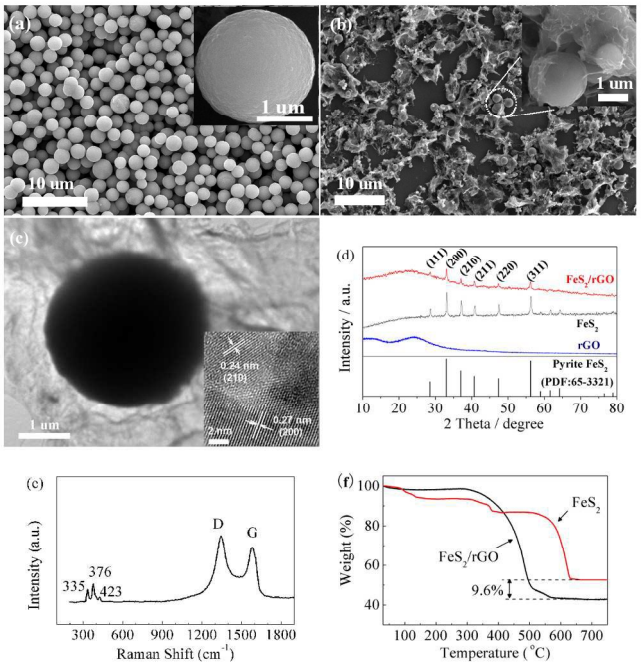

Fig. 2. SEM images of (a) the as-synthesized FeS_2 microspheres and (b) FeS_2 microspheres/rGO composite. (c) TEM and HRTEM (inset) images of FeS_2 microspheres/rGO composite. (d) XRD patterns of rGO, FeS_2 microspheres and FeS_2 microspheres/rGO composite. (e) Raman spectrum of FeS_2 microspheres/rGO. (f) TGA curves of FeS_2 microspheres and FeS_2 microspheres/rGO in oxygen atmosphere.

Electrochemical performance of the FeS_2 microspheres/rGO composite as anode material for LIB was investigated with cyclic voltammetry (CV). Fig. 3a shows representative CV curves of the FeS_2/rGO composite electrode at a scan rate of 0.1 mV s^{-1} between 0.01 and 3 V *versus* Li^+/Li for the first, second and third discharge/charge cycles. Detailed mechanisms for reduction and oxidation of lithium and FeS_2 during discharge/charge have been discussed in previous works.[15-22] In the first cycle, two reduction peaks were at 0.6 and 1.2 V while two oxidation peaks were at 1.8 and 2.5 V. The sharp peak at about 1.2 V in the cathodic sweep corresponds to the reactions: $FeS_2 + 2Li^+ + 2e^- \rightarrow Li_2FeS_2$ and $Li_2FeS_2 + 2Li^+ + 2e^- \rightarrow 2Li_2S + Fe$. The two reactions proceed simultaneously with a single reaction $FeS_2 + 4Li^+ + 4e^- \rightarrow Fe + 2Li_2S$ for the Li^+ has relatively slow diffusion in pyrite FeS_2 at room temperature. The broad peak from 0.6 to 0.01 V is attributed to the formation of a solid electrolyte interlayer (SEI) on the electrode surface which disappears in the following. For the anodic sweep, the peak at 1.8 V is related to the formation of $Li_{2-x}FeS_2$ according to the reactions $Fe + 2Li_2S \rightarrow Li_2FeS_2 + 2Li^+ + 2e^-$ and $Li_2FeS_2 \rightarrow Li_{2-x}FeS_2 + xLi^+ + xe^-$, and the peak at 2.5 V further to the formation of FeS_y and S according to the reaction $Li_{2-x}FeS_2 \rightarrow FeS_y + (2-y)S + (2-x)Li^+ + (2-x)e^-$. After the first cycle, the reduction peaks changed to two peaks at about 2.0 and 1.4 V which correspond to the conversion reactions $FeS_y + (2-y)S + 2Li^+ + 2e^- \rightarrow Li_2FeS_2$ (2.0 V) and $Li_2FeS_2 + 2Li^+ + 2e^- \rightarrow Fe + 2Li_2S$ (1.4 V), respectively. This indicates an irreversible phase change due to the formation of S and Li_2S during the discharge/charge process. Moreover, there is a slight change for the subsequent anodic sweep in the peaks position from the second cycle, implying excellent electrochemical reversibility.

Fig. 3b shows the cycling performance of the FeS_2 microspheres/rGO composite between 0.01 V and 3 V at a current density of 890 mAh g^{-1} (1C). The discharge capacity is 763 mA h g^{-1} at the 1st cycle, while this value decreases to 557 mA h g^{-1} at the 20th cycle. The discharge capacity of the composite during the initial 20 cycles could be attributed to the formation of SEI layer and the irreversible reaction between Li, FeS_2 and rGO. It is interesting that the capacity increases from 557 mA h g^{-1} to 970 mA h g^{-1} within 250 cycles with a high coulombic efficiency of 99.9%. The phenomenon of the gradually increasing capacity in the initial cycles is normally observed for transition metal compounds,[3-5] which is attributed to the reversible formation of a polymeric gel-like film originating from kinetic activation in the electrode. Additionally, there is a long active period for the electrolyte penetrating into the inner part of the FeS_2 microspheres, making the inner part also involved in the conversion reactions. From the 250th cycle upwards, the capacity shows a relatively mild change: the discharge capacity is ~970 mA h g^{-1} after 300 cycles, which is much higher than the theoretical maximum of graphite (i.e. 372 mA h g^{-1}) and also slightly higher than the theoretical value (~890 mA h g^{-1}) of FeS_2. The high capacities

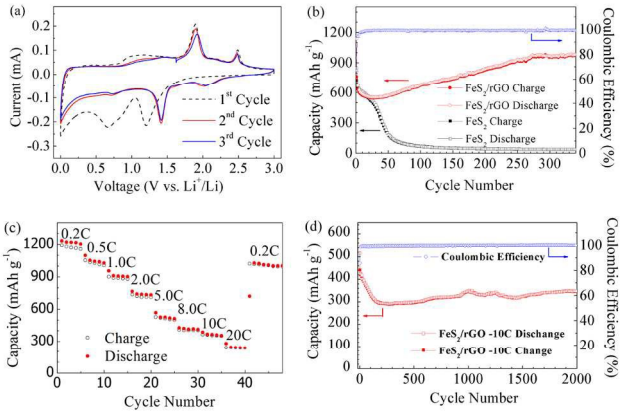

Fig. 3. (a) Cyclic Voltammetry of the FeS_2 microspheres/rGO electrode. (b) Comparison of the cycling performance of the FeS_2 microspheres/rGO and FeS_2 electrode, and corresponding CE of the FeS_2 microspheres/rGO electrode. (c) Rate performance of the FeS_2 microspheres/rGO electrode at various current densities. (d) Cycling performance of the FeS_2 microspheres/rGO electrode at 10C rate.

could be attributed to synergistic effects, including the reversible formation/dissolution of polymeric gel-like film resulted from electrolyte degradation, which is often observed in transition metal compounds, and the insertion of lithium ions into interfacial storage and acetylene black. To study the effect of rGO, the cycling performance of the pristine FeS_2 microspheres was also evaluated (Fig. 3b) at the same current density of 890 mA g^{-1}. However, the discharge capacity of pristine FeS_2 microspheres decreases quickly to less than 100 mAh g^{-1} within 50 cycles. It is clear that the cycling stability of the FeS_2 microspheres/rGO composite is significantly enhanced by the rGO.

Rate performance and high rate cycling stability are crucial to high power batteries applications. Fig. 3c shows the discharge/charge curves observed at various current rates between 0.01 and 3.0 V. It shows fifth-cycle discharge capacities of around 1202 mAh g^{-1} (0.2C), 1027 mAh g^{-1} (0.5C), 901 mAh g^{-1} (1.0C), 732 mAh g^{-1} (2.0C), 512 mAh g^{-1} (5.0C), 360 mAh g^{-1} (10C), and 237 mAh g^{-1} (20C). The FeS_2/rGO composite electrode exhibits a good cycling response at various rates. Even when the current reaches 10C (8900 mA g^{-1}) the electrode can still maintain a capacity 380 mAh g^{-1}. Significantly enhanced cycling stability was achieved over 2000 cycles for cycling at 10C with the voltage range of 0.01-3.0 V versus Li/Li^+, as shown in Fig. 3d. The FeS_2/rGO composite has an initial discharge/charge capacity of 510 and 440 mAh g^{-1}, respectively, with a CE of 86%. The discharge capacity of FeS_2/rGO drops lowest to 290 mAh g^{-1} and the CE increase to 99% to the next 300 cycles, then rebounds and stabilizes. The discharge capacities at 2000 cycles retain 347 mAh g^{-1}, with a CE of 99.8%. This outstanding stable cycle performance of FeS_2 microspheres/rGO composite is mainly due to good dispersion of FeS_2 particles with graphene wrapping on the surface. The above encouraging results show that FeS_2/rGO composite synthesized in this work could be potentially used as a high power density material in lithium-ion batteries.

Electrochemical impedance spectroscopy (EIS) was used to evaluate the interfacial charge transfer capability of FeS_2/rGO electrode. Fig. 4a shows Nyquist plots of the as-prepared cell, after 1, 25, 100 cycles at 1.0 C rate. The diameter of the semicircle at high frequency, which is attributed to the charge-transfer reaction at the electrolyte/electrode interface, is decreased with discharge/charge process. This means an increased electrical conductivity of the electrode as well as an enhanced electrochemical activity of the FeS_2/rGO electrode along with the discharge/charge process, which results in an increased capacity. The reduction in electrical resistance might be attributed to the synergistic effect of the decrease of the FeS_2 particles size and increase of the rGO conductivity upon cycling, similar to the phenomenon found in many grapheme-based composites.[40, 41] The size reduction of particles which was further confirmed by TEM of the cycled FeS_2/rGO electrode, signifies the enhanced electrical conductivity between rGO and FeS_2 particles.

TEM and XRD were performed on cycled FeS_2/rGO composite to evaluate the morphology and structure changes after discharge/charge cycles. Fig. 4b shows the XRD diffraction pattern of the FeS_2/rGO composite after 2000 cycles at 10C rate. The cycled FeS_2/rGO shows a different XRD pattern to the as-prepared FeS_2/rGO, the diffraction peaks can be indexed to the pyrrhotite $Fe_{1-x}S$ (JCPDF card No. 20-0534), which is analogous to the previous reports.[9,12] The composite morphology and crystal structure are further studied by TEM as shown in Fig. 4c. The Fig. 4d shows a HRTEM image in which the lattice space of 0.180, 0.208 and 0.239 nm match with (309), (2014) and (2010) planes of the pyrrhotite $Fe_{1-x}S$, respectively. This indicates that the FeS_2 microspheres are broken into nanoparticles wrapped by graphene. According to recent research,[11-13] at room temperature Li^+ has relatively slow diffusion into pyrite FeS_2, it is evident that pyrite FeS_2 is not reformed at high charge, therefore the final reduction and oxidation may proceed with the reactions between Li^+ and pyrrhotite $Fe_{1-x}S$ at a high rate discharge/charge process. The reaction mechanism of pyrite FeS_2 at high rate cycle process still needs further investigations.

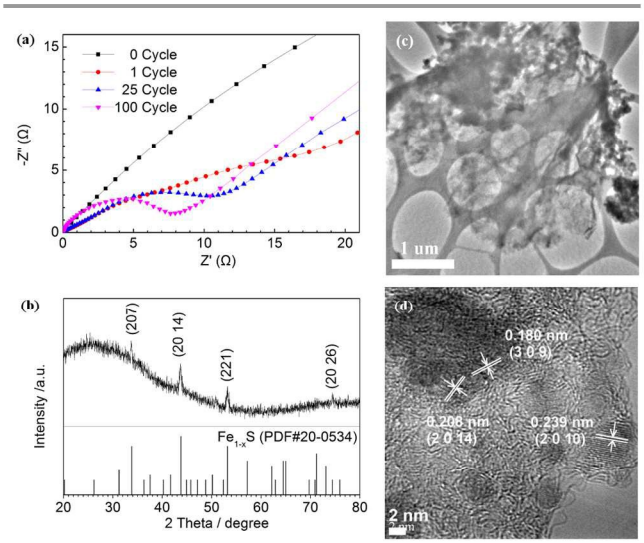

Fig. 4. (a) EIS of the FeS_2 microspheres/rGO electrode after 0-100 cycles. (b) XRD pattern, (c) TEM, and (d) HRTEM of microspheres FeS_2/rGO after 2000 cycles at 10C.

Conclusions

In conclusion, pyrite FeS_2 microspheres wrapped with reduced GO sheets were synthesized *via* a facile solvothermal method. Owing to the excellent conductivity, large effective contact surface area, and superior effectively polysulfide preservation of graphene which wrapped on the surface of the FeS_2, the as-prepared FeS_2/rGO composite exhibit significantly enhanced electrochemical cycling stability and rate performance. This composite exhibited an impressive capacity of ~970 mA h g^{-1} after 300 cycles at a current density of 890 mAh g^{-1} (1.0C). Moreover, it retains a capacity of ~380 mAh g^{-1} even at a high current density of 8900 mAh g^{-1} after 2000 cycles, indicating its potential applications for LIBs with long cycle life and high power density.

Acknowledgements

This project has been financially supported by National Natural Science Foundation of China (No.51272217, 51302238), Guangdong Innovative and Entrepreneurial Research Team Program (No.2013C090), and Collaboration Project of City University of Hong Kong and Shenzhen Huawei (YB2012090343).

Notes and references

[a] Center of Super-Diamond and Advanced Films (COSDAF), City University of Hong Kong, Hong Kong SAR, P.R. China.
[b] Department of Physics and Materials Science, City University of Hong Kong, Hong Kong SAR, P.R. China.
[c] Department of Applied Physics, College of Science, Nanjing University of Posts & Telecommunications, Nanjing, P.R. China.
[d] School of Energy and Environment, City University of Hong Kong, Hong Kong SAR, P.R. China.
[e] Functional Thin Films Research Center, Shenzhen Institutes of Advanced Technology, Chinese Academy of Sciences, Shenzhen, P.R. China.
[*] E-mail: Y.B. Tang: tangyb@siat.ac.cn; C.S. LEE: apcslee@cityu.edu.hk;

1 D. Rickard and G. W. Luther III, *Chem. Rev.,* 2007, **107**, 514.
2 C. Wadia, A. P. Alivisatos and D. M. Kammen, *Environ. Sci. Technol.*, 2009, **43**, 2072.
3 J. Cabana, L. Monconduit, D. Larcher and M. R. Palacín, *Adv. Mater.*, 2010, **22**, E170.
4 G. L. Henriksen and A. N. Jansen, in *Handbook of batteries*, McGraw-Hill, New York 2002.
5 M. S. Whittingham, *Chem. Rev.*, 2004, **104**, 4271.
6 L. Li, M. Caban-Acevedo, S. N. Girard and S. Jin, *Nanoscale*, 2014, **6**, 2112.
7 G. Henriksen and D. Vissers, *J. Power Sources*, 1994, **51**, 115.
8 T. A. Yersak, H. A. Macpherson, S. C. Kim, V. D. Le, C. S. Kang, S. B. Son, Y. H. Kim, J. E. Trevey, K. H. Oh, C. Stoldt and S. H. Lee, *Adv. Energy Mater.*, 2013, **3**, 120.
9 T. S. Yoder, M. Tussing, J. E. Cloud and Y. G. Yang, *J. Power Sources*, 2015, **274**, 685.
10 B. Wu, H. Song, J. Zhou and X. Chen, *Chem. Commun.*, 2011, **47**, 8653.
11 C. Xu, Y. Zeng, X. Rui, N. Xiao, J. Zhu, W. Zhang, J. Chen, W. Liu, H. Tan, H. H. Hng and Q. Yan, *ACS Nano*, 2012, **6**, 4713.
12 S. B. Son, T. A. Yersak, D. M. Piper, S. C. Kim, C. S. Kang, J. S. Cho, S. S. Suh, Y. U. Kim, K. H. Oh and S. H. Lee, *Adv. Energy Mater.*, 2014, **4**, 1300961.
13 J. Liu, Y. Wen, Y. Wang, P. A. V. Aken, J. Maier and Y. Yu, *Adv. Mater.*, 2014, **26**, 6025.
14 A. M. Golsheikh, N. Huang, H. Lim, C. Chia, I. Harrison and M. Muhamad, *Chem. Eng. J.*, 2013, **218**, 276.
15 D. Golodnitsky and E. Peled, *Electrochim. Acta*, 1999, **45**, 335.
16 R. Fong, J. R. Dahn and C. H. W. Jones, *J. Electrochem. Soc.*, 1989, **136**, 3206.
17 Y. Shao-Horn, S. Osmialowski and Q. Horn, *J. Electrochem. Soc.*, 2002, **149**, A1547.
18 X. Wang, Q. Xiang, B. Liu, L. Wang, T. Luo, D. Chen and G. Shen, *Sci. Rep.*, 2013, **3**, 2007.
19 T. Evans, D. M. Piper, S. C. Kim, S. S. Han, V. Bhat, K. H. Oh and S. H. Lee, *Adv. Mater.*, 2014, **26**, 7386.
20 Y. X. Yin, S. Xin, Y. G. Guo and L. J. Wan, *Angew. Chem. Int. Edit.*, 2013, **52**, 2.
21 X. L. Ji, K. T. Lee and L. F. Nazar, *Nat. Mater.*, 2009, **8**, 500.
22 Y. Yang, G. Yu, J. J. Cha, H. Wu, M. Vosgueritchian, Y. Yao, Z. Bao and Y. Cui, *ACS Nano*, 2011, **5**, 9187.
23 L. W. Ji, M. M. Rao, H. M. Zheng, L. Zhang, Y. C. Li, W. H. Duan, J. H. Guo, E. J. Cairns and Y. G. Zhang, *J. Am. Chem. Soc.*, 2011, **133**, 18522.
24 C. X. Zu and A. Manthiram, *Adv. Energy Mater.*, 2013, **3**, 1008.
25 H. L. Wang, Y. Yang, Y. Y. Liang, J. T. Robinson, Y. G. Li, A. Jackson, Y. Cui and H. J. Dai, *Nano Lett.*, 2011, **11**, 2644.
26 S. Eversa and L. F. Nazar, *Chem. Commun.*, 2012, **48**, 1233.
27 N. W. Li, M. B. Zheng, H. L. Lu, Z. Z. Hu, C. H. Shen, X. F. Chang, G. B. Ji, J. M. Cao and Y. Shi, *Chem. Commun.*, 2012, **48**, 4106.
28 Y. L. Cao, X. L. Li, I. A. Aksay, J. Lemmon, Z. M. Nie, Z. G. Yang and J. Liu, *Phys. Chem. Chem. Phys.*, 2011, **13**, 7660.
29 J. Z. Wang, L. Lua, M. Choucairc, J. A. Stridec, X. Xua and H. K. Liu, *J. Power Sources*, 2011, **196**, 7030.
30 W. D. Qiu, J. Xia, H. M. Zhong, S. X. He, S. H Lai and L. P. Chen, *Electrochim. Acta*, 2014, **137**, 197.
31 W. D. Qiu, J. Q. Jiao, J. Xia, H. M. Zhong and L. P. Chen, *RSC Adv.*, 2014, **4**, 50529.
32 W. D. Qiu, J. Xia, S. X. He, H. J. Xu, H. M. Zhong and L. P. Chen, *Electrochim. Acta*, 2014, **117**, 145.
33 W. D. Qiu, J. Q. Jiao, J. Xia, H. M. Zhong and L. P. Chen, *Chem. Eur. J.*, 2015, 21, 4359.
34 X. Huang, X. Qi, F. Boey and H. Zhang, *Chem. Soc. Rev.*, 2012, **41**, 666.
35 W. S. Hummers and R. E. Offeman, *J. Am. Chem. Soc.*, 1958, **80**, 1339.
36 D. C. Marcano, D. V. Kosynkin, J. M. Berlin, A. Sinitskii, Z. Sun, A. Slesarev, L. B. Alemany, W. Lu and J. M. Tour, *ACS Nano*, 2010, **4**, 4806.
37 J. Xu, H. T. Xue, X. Yang, H. X. Wei, W. Y. Li, Z. P. Li, W. J. Zhang and C. S. Lee, *Small*, 2014, **10**, 4754.
38 M. Cabán-Acevedo, M. S. Faber, Y. Tan, R. J. Hamers and S. Jin, *Nano Lett.*, 2012, **12**, 1977.
39 L. Malard, M. Pimenta, G. Dresselhaus and M. Dresselhaus, *Phys. Rep.*, 2009, **473**, 51.
40 Y. Sun, X. Hu, W. Luo and Y. Huang, *ACS Nano*, 2011, **5**, 7100.
41 X. S. Zhou, L. J. Wan and Y. G. Guo, *Adv. Mater.*, 2013, **25**, 2152.